4D printing with spin-crossover polymer composites

Mario Piedrahita-Bello, José Elias Angulo-Cervera, Rémi Courson, Gábor Molnár, Laurent Malaquin, Christophe Thibault, Bertrand Tondu, Lionel Salmon, Azzedine Bousseksou

COMMUNICATION

4D Printing with Spin-Crossover Polymer Composites

Mario Piedrahita-Bello,[a,b] José Elias Angulo Cervera,[a,b] Rémi Courson,[b] Gábor Molnár,[a] Laurent Malaquin,[b] Christophe Thibault,[b] Bertrand Tondu,[b] Lionel Salmon,[*,a] Azzedine Bousseksou[*,a]

Received 00th January 20xx,
Accepted 00th January 20xx

DOI: 10.1039/x0xx00000x

A stereolithographic 3D printing method was used to fabricate spin crossover-polymer composite materials with various shapes and sizes (up to several cm). The thermomechanical properties of the polymer and the stiumuli-responsive properties of the filler are preserved in the composite - affording for a new approach of 4D printing.

Three-dimensional (3D) printing, also called additive manufacturing, consists to fabricate objects from a 3D computer model by joining materials, as opposed to subtractive/formative manufacturing approaches. In the past decades, numerous 3D printing technologies have been developed to pattern complex shapes with various object sizes, printing resolution and fabrication speed.[1-2] In general, 3D printing is achieved layer-by-layer using either ink deposition or laser-writing process, though other approaches are also employed. Yet, in each case, one of the main bottlenecks is the limited number of advanced materials, which can be 3D printed for specific applications.[3]

In this context, 3D printing of smart, stimuli responsive materials has received increasing attention in the past few years.[4-6] These materials allow for the evolution of the shape and/or functionality of the 3D printed object with time when exposed to a stimulus, such as light irradiation, solvents, electric/magnetic fields, pH or heat. To differentiate these objects from "static" 3D printed structures, they were coined with the term "4D printing", wherein the fourth dimension refers to time.[7] Among the different materials used for 4D printing, shape memory polymers, liquid crystal elastomers and hydrogels have been the most popular, with associated polyjet printing and extrusion printing methods. The envisioned applications of 4D printing comprise smart valves, grippers, drug delivery systems, self-healing and adaptive structures, soft robots and so forth.[4-7]

A straightforward way to introduce novel functionalities and/or enhance properties of existing 3D printing materials is the use of printable polymer composites.[8] This approach has allowed, for example, to reinforce the polymer matrix, to improve/adjust its dielectric permittivity, electrical conductivity, thermal diffusivity/stability, hydrophilicity as well as to confer it with magnetic or piezoelectric properties. Perhaps not surprisingly, polymer composites have received also much attention for 4D printing applications.[5] Obviously, the key challenge here is to ensure 3D printability of the composite material without compromising the original properties of the constituents.

In this Communication, we describe a novel approach for 4D printing, based on spin crossover - polymer nanocomposites. Spin crossover (SCO) is a phenomenon that occurs in some transition metal complexes wherein the spin state of the complex changes reversibly from the low spin (LS) to the high spin (HS) state due to an external stimulus such as a variation of temperature/pressure, magnetic or electric fields, vapour adsorption or light irradiation.[9-10] The spin crossover effect is accompanied by a significant change of magnetic, optical, electrical and mechanical properties. The latter property is used in SCO based mechanical actuators, wherein the volumetric strain can reach 15 %.[11] The advantages of SCO compounds with respect to other smart materials for the elaboration of composite actuators are (1) the high work density, (2) the fast switching, (3) the possibility to tune the transition temperature and (4) multifunctionality. For our work, a key asset is the compatibility of SCO materials with various polymers, which has already been advantageously used for the fabrication of SCO-polymer composite actuators.[12-15]

Recently, some of us have reported the direct laser fabrication of 2D and 3D architectures (scalable up to 500 cm^3) with micrometric feature resolution using a single-photon absorption stereolithographic methodology (SLA), based on the photopolymerization of a resin.[16] The effective polymerization

[a] *Laboratoire de Chimie de Coordination, CNRS UPR 8241, 205 route de Narbonne, F–31077 Toulouse, France. E_mail : lionel.salmon@lcc-toulouse.fr, azzedine.bousseksou@lcc-toulouse.fr*

[b] *Laboratoire d'Analyse et d'Architecture des Systèmes, CNRS UPR 8001, 7 avenue du Colonel Roche, F–31400 Toulouse, France.*

Electronic Supplementary Information (ESI) available: Additional sample characterization details. See DOI: 10.1039/x0xx00000x

depth in the material allows to easily write both in thick (maximum tested 100 µm) and thin (minimum tested 10 µm) layers as well as to realize 3D architectures including true freestanding structures without the need of sacrificial supports. Here we use this methodology to 3D print SCO nanocomposites. First, a powder sample of the $[Fe(NH_2trz)_3]SO_4$ (trz = 1,2,4-triazole) spin crossover complex was prepared using a slightly modified version of the synthesis proposed in ref. 17. This complex has been chosen because of the important volume change of its unit cell (ca. 9%) upon the SCO phenomenon, its good cyclability and weak absorption at the SLA laser wavelength (405 nm). Figure S1 in the Electronic Supporting Information (ESI) shows two consecutive cycles of the thermal variation of the magnetic susceptibility. Subsequent to a first 'run-in' cycle, the compound presents stable spin crossover properties with transition temperatures of $T_{1/2}^{\uparrow}$ = 67°C and $T_{1/2}^{\downarrow}$ = 56°C for the heating and cooling modes, respectively, denoting a hysteresis loop of ca. 9°C width. Transmission electron microscopy reveals that the microcrystalline powder consists of ca. 1-2 µm long rod-shaped particles (see Fig. S1). Homogeneous suspensions of the particles were obtained by mechanically mixing the powder sample (up to 20 wt%) with the commercial DS-3000 photosensitive polymer used for 3D printing. The SLA setup (Fig. 1) consists of galvanometric mirrors, which move the laser beam (20 µm diameter) along the x and y directions with a maximum writing speed of 6400 mm/s. The sample holder and the tank are mounted on a z-axis moving stage, which can ensure a minimum layer thickness of 10 µm. The maximum printed object volume is 15 (x) × 15 (y) × 10 (z) cm^3. All the structures produced in this work were obtained layer-by-layer using a raster scan filling procedure.

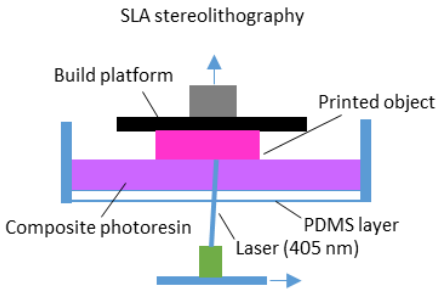

Fig. 1. Scheme of the 3D fabrication setup.

We started by 3D printing uniform structures with homogeneous distribution of the SCO load within the whole object. This required the assessment of the adequate laser dose to complete the photo-polymerization for each sub-layer for a selected thickness and selected SCO loading. Whatever the laser dose used, above ca. 15-20 wt% SCO load it was not possible to obtain a stable multilayer film as the sample became too brittle (see Fig. S2). A good compromise consisted in using 15 wt% SCO complex with 5800 mm/s writing speed, z-slicing set at 30 µm/layer and a hatching of 30 µm to avoid overexposure and reduce the overall fabrication time (15 min for a 1 mm thick pattern). To remove the unexposed materials the sample was developed in an isopropanol bath under sonication for 15 minutes. Using this procedure, 2D and 3D shapes (square, triangle, spring, dog bone, etc.) were printed with various thicknesses (from 100 to 1000 µm) and sizes (up to 3 cm long) (Fig. 2). The most complex 3D structures we fabricated are helical springs of 6,6 mm length, 4,2 mm diameter, 300 µm wire diameter, pitch size of 800 µm and coil angle of 18 degrees. These springs were fabricated with supporting bars of 500 µm, which were eventually removed. Clearly, 3D printing allows us to obtain SCO materials with shapes, which would be extremely difficult, if not impossible, to obtain by other fabrication methods.

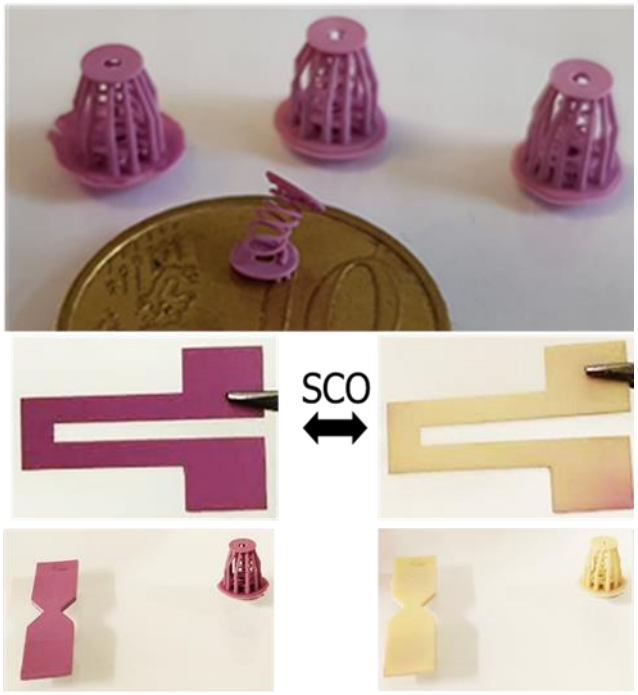

Fig. 2. 3D printed SCO-polymer composite objects. Upon heating above ca. 80 °C a reversible colour change occurs between the LS (violet) and HS (light-yellow) states.

Heating of the structures by a heat gun allowed for a visual confirmation of the SCO phenomenon and its reversibility (Fig. 2). For a more detailed assessment of the properties of the composite materials, we carried out differential scanning calorimetry (DSC) and thermogravimetric (TG) measurements, as well as thermomechanical analysis (TMA) coupled with optical reflectivity detection (see the ESI for experimental details). As shown in Fig. S1, the spin transition in the composite occurs at slightly lower temperatures ($T_{1/2}^{\uparrow}$ = 65°C and $T_{1/2}^{\downarrow}$ = 54°C), which might be ascribed to the elastic confinement in the polymer matrix.[18] To control the thermal stability of the printed devices at the actuation temperatures, differential scanning calorimetry (DSC) and thermogravimetric analysis (TGA) were performed on both the composite, the pure complex and the pure DS3000 resin (see Fig. S3 in the ESI). These thermal analyses show that SCO occurs at a temperature well below any crystalline transition of the polymer matrix, and that the composite retains its stability up to 220°C, thus ensuring that actuation does not interfere with the properties of the polymer

matrix (Fig. S3). From the TMA analysis, the Young's modulus of the 15 wt% SCO composite (1.7 ± 0.2 GPa) at room temperature is comparable with that of the pure polymer matrix (1.5 ± 0.2 GPa). Upon heating, one can observe a similar decrease of the Young's modulus (ca. 0.2 GPa at 90 °C) in the two samples, but a detailed tracking reveals in the SCO composite a discontinuity of the Young's modulus around the spin transition temperatures – the HS phase being considerably softer (Fig. 3).

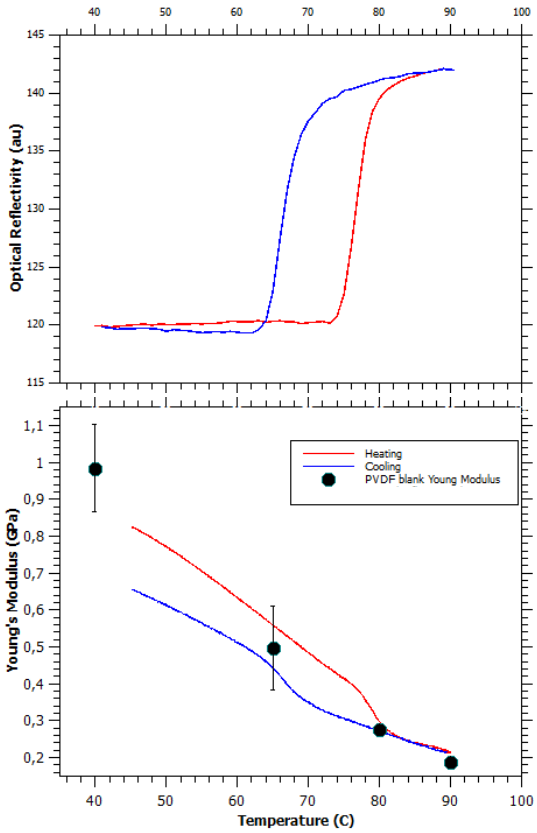

Fig. 3. Simultaneous optical reflectivity – thermomechanical analysis of the 3D printed SCO-polymer composite. The Young's modulus of the pure polymer is also shown at selected temperatures.

To demonstrate 4D printing we fabricated a 3 cm long bimorph architecture consisting of two stacks: the pure DS-3000 polymer and the SCO-polymer composite. Such bimorph structures are commonly used for actuation magnification, because the different expansion of the two strata allows for large amplitude bending movement.[15] A common pitfall in this mechanism, however, is delamination and our efforts were focused therefore on ensuring strong adhesion between the two stacks. For the 3D printing of bimorphs, the tank was divided by a PDMS wall into two area. First, the pure DS-3000 stack (90 µm) was printed at 200 mm/s writing speed to ensure tight adhesion with the build platform, setting the z-slicing at 30 µm/layer and 60 µm of hatching, for an overall fabrication time of around 7 minutes. Then the build table was removed and put into an isopropanol bath to remove the uncrosslinked polymer. The build table was then replaced into the 3D printer to continue the second part of the printing with the SCO material (thickness of 150 µm) stored in the other part of the tank. In this case, the z-slicing and the hatching parameters were fixed to 30 µm. In order to obtain strong adhesion between the layers of pure DS-3000 and the composite layers containing SCO material it is necessary to elaborate the first SCO composite layers under the same high-exposure conditions used for the elaboration of the pure DS-3000 layers. (To illustrate this pivotal issue, Figure S2 shows a bimorph obtained using lower exposure.) Afterwards, in order to reduce the fabrication time, the writing speed was increased to 400 mm/s. Figure 4 shows SEM images of the transversal section of a 3D printed bimorph pattern containing 15 wt% SCO filler. (See coupled EDX analysis in Fig. S4.). We can clearly discern the interface between the smooth, nude DS-3000 stack and the rough SCO/DS-3000 composite stack containing well dispersed particles of the SCO compound. Note the good continuity between the two layers, which is an indispensable feature to avoid the delamination and to optimise the performance of the bimorph actuator.

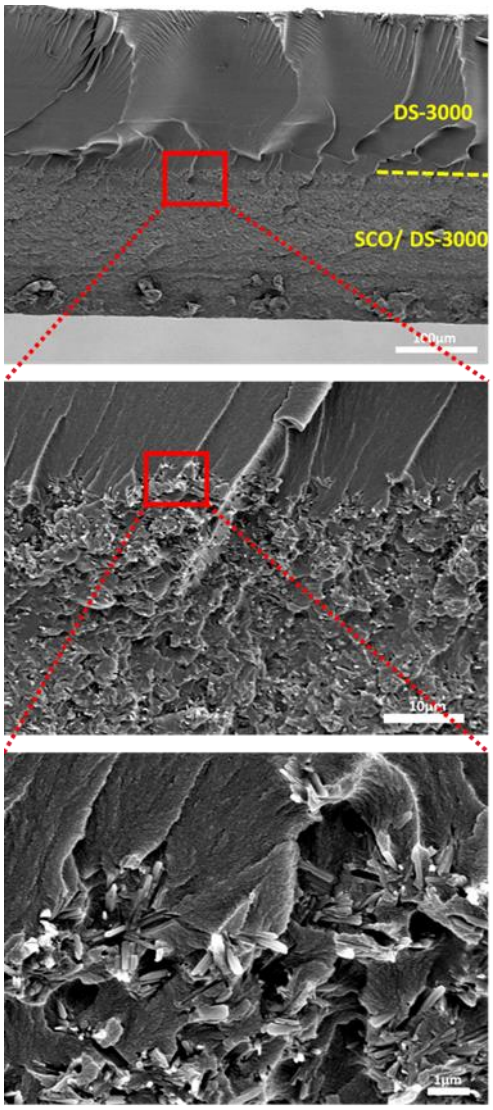

Fig. 4. SEM images showing at different magnifications the interface of the neat polymer and polymer composite stacks in bimorph objects.

The thermal expansion coefficients of the two strata are similar, therefore one expects significant bending chiefly around the spin transition temperatures (Figures 5 and S5). Figure 5a shows

side-view optical images of a 1 mm thick bimorph structure at two temperatures below (pink) and above (colourless) the spin transition temperature. As expected, for increasing aspect ratios, the bending amplitude also increased. The tip displacement for a thin (0.24 mm) sample upon heating and cooling between 15 and 120 °C is depicted in Figure 5b. One can note the brusque movement associated with the spin transition. The tip displacement for this 30-mm-long bimorph is ca. 4.5 mm, denoting a displacement (D)-to-length (L) ratio of D/L = 0.15. This effect was successfully repeated during twenty thermal cycles for both aspect ratios. In order to use the classical bilayer model to determine the mechanical and actuating properties of our composite, a simple rectangular bilayer object was fabricated (Fig S6). Using the classical Timoshenko model for bilayer actuators, the total strain of the active layer caused by the SCO phenomenon was calculated.[19,12] The linear strain of the active layer (ΔL/L) is 0.33 %. Using this value, the volumetric work density of the actuator could be estimated as W/V = 1.5 mJ·cm^{-3}. This value determines the maximum amount of work per unit volume that an actuator can perform. (Further details on these calculations can be found on the SI.) We have also included in the SI a table comparing different bending type polymer-based, soft actuators. The actuating performance of the present 3D printed actuator falls between that of different systems, but remains perfectible even in comparison with other SCO-based systems. In particular, the use of 3D resins with higher Young's modulus and SCO compounds with lower transition temperature could bring significant improvements.

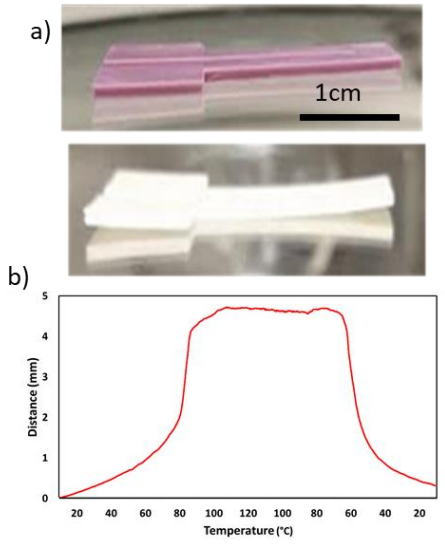

Fig. 5. (a) Colour change and associated bending of a bimorph actuator (850 µm active layer and 150 µm inactive layer) upon the SCO. (b) Actuation cycle of a bimorph actuator (150 µm active layer and 90 µm inactive layer) upon heating and cooling.

Conclusions

Using a stereolithographic approach in conjunction with spin crossover-polymer composites, we have 3D printed various stimuli-responsive mono- and bimorph architectures with sizes up to several cm and structural details down to the 80 µm scale. The objects display good thermal and mechanical properties and afford for reversible mechanical actuation generated by the volume change accompanying the spin crossover phenomenon. The fabrication process developed here is straightforward, versatile and enables the creation of arbitrary planar and three-dimensional geometries, which are otherwise not accessible using spin crossover complexes. This work widens the restricted choice of materials for 4D printing and opens up prospects for a range of applications including grippers, moving parts in microfluidics, drug delivery, adaptive optics, and so forth.

Acknowledgment

We thank financial support from the Federal University of Toulouse/ Région Occitanie (PhD grant of MPB), the Agence Nationale de la Recherche (ANR-19-CE09-0008-01), the French RENATECH network, supported as part of the MultiFAB project funded by FEDER European Regional Funds and Région Occitanie (Grant No.16007407/MP0011594) and the European Commission (H2020-MSCA-RISE-2016, SPINSWITCH, No.734322 and H2020-NMBP-PILOTS-2017, HoliFAB, No.760927).

Notes and references

1 T. D. Ngo, A. Kashani, G. Imbalzo, K. T. Q. Nguyen and D. Hui, *Composites Part B*, 2018, **143**, 172.
2 M. Vaezi, H. Seitz and S. Yang, *Int. J. Adv. Manuf. Tech.*, 2013, **67**, 1721.
3 J.-Y. Lee, J. An and C. K. Chua, *Appl. Mater. Today*, 2017, **7**, 120.
4 F. Momeni, S. M. Hassani, X. Liu and J. Ni, *Materials and Design*, 2017, **122**, 42.
5 Z. X. Khoo, J. E. M. Teoh, Y. Liu, C. K. Chua, S. Yang, J. An, K. F. Leong and W. Y. Yeong, *Virtual and Physical Prototyping*, 2015, **10**, 103.
6 X. Kuang, D. J. Roach, J. Wu, C. M. Hamel, Z. Ding, T. Wang, M. L. Dunn and H. J. Qi, *Adv. Funct. Mater.*, 2019, **29**, 1805290.
7 S. Tibbits, *Archit. Des.*, 2014, **84**, 116.
8 X. Wang, M. Jiang, Z. Zhou, J. Gou and D. Hui, *Composites Part B*, 2017, **110**, 442.
9 *Spin Crossover in Transition Metal Compounds I-III*, ed. P. Gütlich and H. A. Goodwin, Springer, Berlin, 2004, vol. 233–235.
10 A. Bousseksou, G. Molnar, L. Salmon and W. Nicolazzi, *Chem. Soc. Rev.*, 2011, **40**, 3313.
11 M. D. Manrique-Juárez, S. Rat, L. Salmon, G. Molnár, C. M. Quintero, L. Nicu, H. J. Shepherd and A. Bousseksou, *Coord. Chem. Rev.*, 2016, **308**, 395.
12 H. J. Shepherd, I. A. Gural'skiy, C. M. Quintero, S. Tricard, L. Salmon, G. Molnár and A. Bousseksou, *Nat. Commun.*, 2013, **4**, 2607.
13 I. A. Guralskiy, C. M. Quintero, J. S. Costa, P. Demont, G. Molnar, L. Salmon, H. J. Shepherd and A. Bousseksou, *J. Mater. Chem. C*, 2014, **2**, 2949.
14 Y.-C. Chen, Y. Meng, Z.-P. Ni and M.-L. Tong, *J. Mater. Chem. C*, 2015, **3**, 945.
15 M. D. Manrique-Juárez, F. Mathieu, A. Laborde, S. Rat, V. Shalabaeva, P. Demont, O. Thomas, L. Salmon, T. Leichle, L. Nicu, G. Molnár and A. Bousseksou, *Adv. Funct. Mater.*, 2018, **28**, 1801970.
16 P. Juskova, A. Ollitrault, M. Serra, J.-L. Viovy and L. Malaquin, *Anal. Chim. Acta*, 2018, **1000**, 239.

17 L. G. Lavrenova, O. G. Shakirova, V. N. Ikorskii, V. A. Varnek, L. A. Sheludyakova and S. V. Larionov, *Russian J. Coord. Chem.*, 2003, **29**, 22.
18 A. Tissot, C. Enachescu and M.-L. Boillot, *J. Mater. Chem.*, 2012, **22**, 20451.
19 S. P. Timoshenko, *J. Opt. Soc. Am.* 1925, **11**, 233.